



Automatic for Generating Landmark Mandibular Panoramic Radiography Image

Nur Nafi'iyah^{1,3} Chastine Fatichah^{1*} Darlis Herumurti¹ Eha Renwi Astuti²
Ramadhan Hardani Putra² Agus Subhan Akbar⁴

¹Department of Informatics, Institut Teknologi Sepuluh Nopember, Surabaya, Indonesia

²Department of Dentomaxillofacial Radiology, Faculty of Dental Medicine,
Universitas Airlangga, Surabaya, Indonesia

³Department of Informatics, Universitas Islam Lamongan, Lamongan, Indonesia

⁴Department of Information System, Universitas Islam Nahdlatul Ulama Jepara, Jepara, Indonesia

* Corresponding author's Email: chastine@if.its.ac.id

Abstract: Forensic gender identification based on teeth is needed to identify incomplete victims, only bones and teeth. Previous studies identified gender by manually or semi-automatically measuring mandibular parameters based on landmark points. Gender identification, especially for victims of mass disasters, requires accuracy, so it takes longer, especially if there are many parameters to be measured. In addition, the observer's manual or semi-automatic measurements may give different results. This study proposes a new automatic approach to generate ten mandibular landmark points from panoramic radiographic images for gender identification. We propose a step, namely determining the centroid point of the mandibular image and using linear regression to predict ten mandibular landmark points such as the two condyle, two gonion, four ramus, and two body of the mandible. This study obtained panoramic radiographic images from the Academic Dental Hospital, Universitas Airlangga. We calculated the distance between expert mandibular landmark points and the predicted results to evaluate performance. The prediction of the landmark with the smallest average distance is the lower point of the mandibular body 1 pixel. In comparison, the predicted landmark with the most extended average length is a gonion of 10 pixels.

Keywords: Mandibular landmark generate, Gender identification, Dental panoramic radiography, Automatic, Linear regression.

1. Introduction

The identity of living and dead victims can be examined using teeth or bones. One way to identify individuals using teeth is by comparing postmortem data (results of examining the victim) and antemortem data (data on the victim's previous teeth). Previous research used an automatic identification process, namely inputting a dental radiographic image, comparing it with a dental radiographic dataset, and looking for the most similar one. Or by using a machine learning algorithm or CNN (convolutional neural networks), where features are extracted from dental radiographic images, trained as a model, and tested [1-4]. At the same time, the

feature extraction method used is geometric features. Feature extraction is used for determining landmarks from objects or creating points and producing angles, length and area of the object [5-10]. Before the feature extraction uses geometric features so the image is binary (black and white) to extract the shapes of the image object, there is a segmentation stage. Previous studies related to segmentation included segmentation of the mandibular canal on radiographs [11] and segmentation of each tooth [12]. However, under certain conditions, teeth cannot be used as an identification tool for several reasons. For example, if the victim's dental data is incomplete or the victim is edentulous, an alternative method is needed, namely, using bones [13-14]. One of the bones that can be used for identification is the

mandibular bone. Previous research states that if teeth are unavailable, the mandible bone can be used because the mandible bone is the strongest and largest bone in the face. In addition, several studies have shown that the mandibular bone is more accurate when identifying gender [15]. Identifying the mandibular bone to determine gender can be done by measuring it through radiography. The radiography used is panoramic digital imagery (digital orthopantomography) [16].

Identification using the mandibular bone is part of the primary identification. Identification using the mandibular bone is the main alternative for victims of mass disasters when secondary identification cannot be carried out due to damage to the victim's body so that he cannot be physically identified. However, identifying the mandibular bones requires high accuracy because you must measure many parameters in its application to get accurate results. So far, the process of measuring mandibular parameters is done semi-automatically by determining mandibular landmark points. In several previous studies, the process of deciding mandibular landmark points used the ImageJ application, which was still semi-automatic [17]. Another research is the process of determining mandibular landmark and semilandmark points based on the mandibular contour in the form of point distribution using the CNN method [18]. Research has been carried out to automatically determine the landmark points of cephalometric images for the dental treatment process [19-22]. The main contributions in this research are as follows: automation method generating landmark points mandibular radiography panoramic. The ten mandibular landmark points are generated automatically, i.e., two condyle, two gonion, four ramus, and two body of the mandible.

This paper is structured as follows: Section 1 of the Introduction explains the background of the research. Section 2 Related work explains previous research related to landmark determination. Section 3, Dataset, describes the data used. Section 4, Automatic mandibular landmark generation, describes the proposed automatic process for determining ten mandibular landmark points. Section 5 Results explains the results of the research and experiments. Section 6 Conclusion is the conclusion of the research.

2. Related work

Research related to predicting landmarks on medical images automatically has been carried out on cephalometric images based on Table 1. Previous research determined mandibular landmark and

semilandmark points based on the mandibular contour in the form of point distribution. The results of the point distribution were measured by distance and angle for the CNN process [18]. The difference between our research and previous [18] is that we propose landmark points automatically using linear regression with ten landmark points (two condyle, two gonion, four ramus, and two body of the mandible).

3. Dataset

The panoramic radiograph from the Academic Dental Hospital, Universitas Airlangga, Surabaya, has good quality and has been confirmed by a radiologist. Data from research segmentation [25] is used as input data to determine mandibular landmark points automatically. The radiologist's role is to select a dataset according to the selection criteria. Inclusion criteria include Patients aged 19-70 years; the radiographic quality is good, and the anatomy of the mandible on the radiograph is visible. Exclusion criteria include unclear mandibular appearance, e.g., superimposed condylar and coronoid areas with other anatomic features; Abnormalities in the mandible, e.g., growth disorders; Tumors/cysts; fracture.

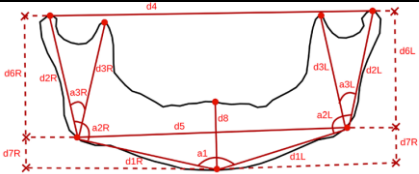
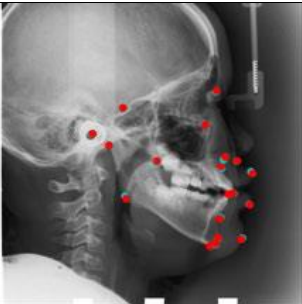
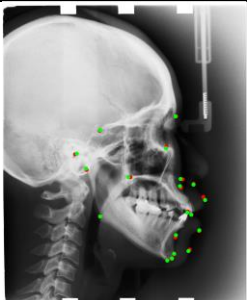
The radiologist's role is to determine 120 panoramic radiographic images and ten mandibular landmark points on panoramic radiography. The ten mandibular landmark points (two condyle, two gonion, four ramus, and two body of the mandible) determined by the expert in Table 2 are examples of four panoramic mandibular radiographic images defined by a radiologist. The panoramic radiographic image the radiologist defines as a landmark is a binary image of the mandible with a size of 224x224. The Health Research Ethics Commission (KKEPK) Faculty of Dentistry, Airlangga University, Surabaya, ethically tested the sample data with certificate No. 043/HRECC. FODM/II/2022. Data 120 we use for training 104 and testing 16 image result of segmentation mandible.

Our dataset includes 120 patients aged 19-70 years and is grouped into five based on research [26]. The distribution of the first group is 19-29 years old, the second group is 30-39 years old, the third group is 40-49 years old, the fourth group is 50-59 years old, and the fifth group is 60-70 years as shown in Table 3.

4. Automatic landmark mandibular generating

The step to get a linear regression model is that the mandibular panoramic radiographic image is cropped and changed to a size of 224x224, the radiologist

Table 1. State-of-the-art automatic point landmark

Method	Research object image	Result point landmark	Evaluation
Deep learning [18]	OPG dataset collected by the School of Medicine and Dentistry of the Universidade de Santiago de Compostela (Spain) with a direct digital panoramic		Accuracy
Deep Regression [19]	Cephalometric X-ray images		Mean Radial Error (MRE) (millimeters)
CephaNet Faster R-CNN [20]	Cephalometric X-ray images. Datasets of the IEEE ISBI 2014 and the IEEE ISBI 2015 challenges		Accuracy
Backbone of ResNet50 [21]	ISBI 2015 Grand Challenge in Dental X-ray Image		Mean Radial Error (MRE) (millimeters)
Deep Convolutional Neural Network (DCNN) [22]	Cephalometric X-ray images. Datasets of the IEEE ISBI 2015 challenges		Error ranges (millimeters)
Random Forest Regression [23]	Cephalometric X-ray images. Datasets of the IEEE ISBI 2014 and the IEEE ISBI 2015 challenges		Mean Radial Error (MRE) (millimeters)

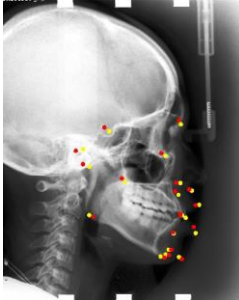
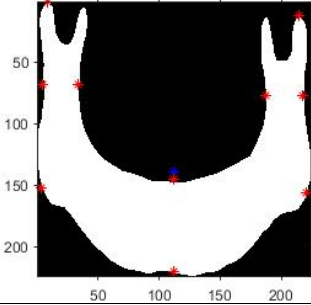
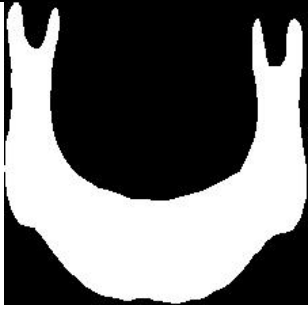
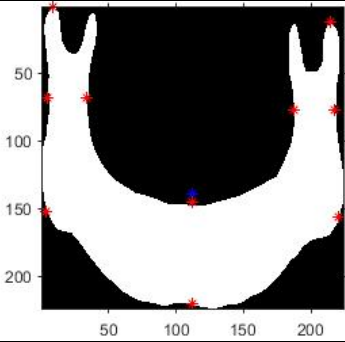
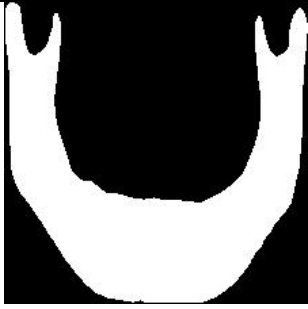
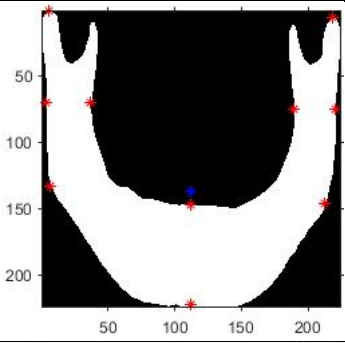
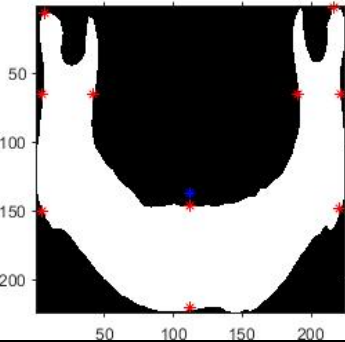
Method	Research object image	Result point landmark	Evaluation
Convolutional Neural Networks (CNN) [24]	ISBI 2015 Grand Challenge in Dental X-ray Image		Average Euclidean distances
Our Proposal	Results of mandibular segmentation on panoramic radiography		Average Euclidean distances

Table 2. Data of landmark mandibular from radiologist's

Input mandibular image	Ground truth mandibular
	
	
	

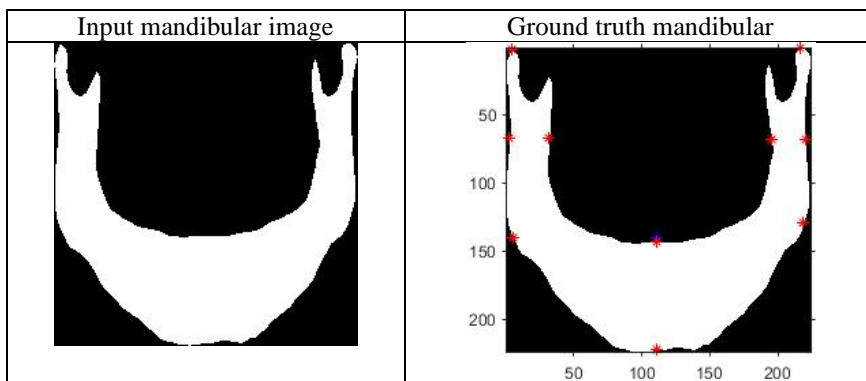


Table 3. Data

Age Group (Year)	Male	Female	Total
19-29	15	14	29
30-39	11	11	22
40-49	12	10	22
50-59	10	11	21
60-70	13	13	26
Total	61	59	120

determines the centroid coordinates (x,y) of the cropped mandibular image size 224×224 and the condyle points left, right, left gonion point, right, left ramus point (2 points), right ramus (2 points), body point bottom, upper. We train the data model of 120 images that have determined the centroid and ten mandibular landmark points. The proposed steps for generating a panoramic radiographic landmark mandibular point are (Fig. 1):

- Read mandibular binary image
- Determining the centroid of each mandibular binary image,
- Determining each mandibular landmark point (two condyle, two gonion, four ramus, and two body of the mandible) of the mandibular binary image using linear regression
- Results landmark mandibular point (Fig. 2). There are four mandibular landmark points in Fig. 2, namely the condyle (a), ramus (b), gonion (c), and body of the mandible (d).

5. Results

We propose generate automatic the (x,y) coordinates of mandibular landmarks. The ten mandibular landmark points determined were the left/right condyle (a), left/right ramus (b), left/right gonion (c), and bottom/top mandibular body (d) (as shown in Fig. 2). To evaluate the prediction model of mandibular landmark points by measuring the actual distance of each mandibular landmark point (two condyle, two gonion, four ramus, and two body of the

mandible) with the predicted results using Euclidian distance (Eq. (1)). The landmark points of the condyle of the mandible (a) (right, left), ramus (b) (right, left), gonion (c) (right, left), and body of the mandible (d) (bottom, upper) were generated using linear regression with input in the form of centroid coordinates (x,y) of the mandibular binary image (as in Algorithm 1).

Based on algorithm 1, determine the points of the left condyle (clx, cly) , right condyle (crx, cry) , left gonion (glx, gly) , right gonion (grx, gry) , bottom mandibular body (mbx, mby) , upper mandibular body (mux, muy) , left ramus (rlx_1, rly_1) , (rlx_2, rly_2) , right ramus (rrx_1, rry_1) , (rrx_2, rry_2) . Following are the results of generating mandibular landmarks using linear regression as shown in Table 5.

$$Error = \sqrt{(x - x')^2 + (y - y')^2} \tag{1}$$

$$MRE = \frac{\sum_{i=1}^n Error_i}{N} \tag{2}$$

$$SDR = \frac{N_a}{N} 100\% \tag{3}$$

To evaluate the proposal's performance, we calculate the ME (mean error) in Eq. (1) [21]; [24] between the landmark mandibular from the radiologist and the proposed method results. Table 4 shows the ME between the panoramic radiographic mandibular landmark point. The radiologist selected the best 120 panoramic radiographic mandibular images. Radiologists defined 120 mandibular of ten landmark mandibular. The radiologist's results of ten landmark mandibular are used as much 104 for training data to create a machine-learning model. Using linear regression, our prediction determined mandibular landmarks in 16 mandibular panoramic radiographic images (Table 5). Algorithm 1 is a linear regression model to determine mandibular landmarks (two condyle, two gonion, four ramus, and two body of the mandible). In research [21], the mean radial

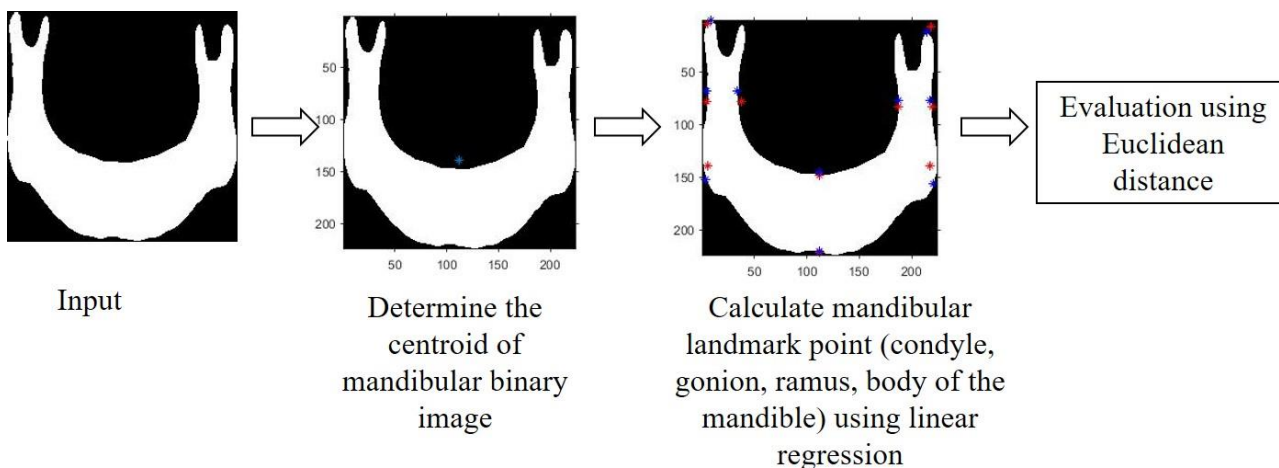


Figure. 1 The proposed method of generate landmark mandibular

Algorithm: 1 a pseudocode to generate mandibular landmarks such as condyle, gonion, ramus, and body mandible.

Input: image mandible binary (I)
 Output: the landmark mandibular such as left/right condyle, left/right gonion, left/right ramus, and bottom/upper body mandible

```

1:  $a = imread(I);$ 
2:  $x, y = centroid(a);$ 
3:  $clx = 15.87 - 0.09x;$ 
4:  $cly = 12.79 - 0.07y;$ 
5:  $crx = 219.39 - 0.02x;$ 
6:  $cry = -111.19 + 0.85y;$ 
7:  $glx = -52.34 + 0.52x;$ 
8:  $gly = 161.91 - 0.17y;$ 
9:  $grx = 199.42 + 0.15x;$ 
10:  $gry = 111.77 + 0.2y;$ 
11:  $mbx = 6.03E - 14 + x;$ 
12:  $mby = 216.47 + 0.03y;$ 
13:  $mux = 6.03E - 14 + x;$ 
14:  $muy = 143.19 + 0.03y;$ 
15:  $rlx_1 = -32.97 + 0.34x;$ 
16:  $rly_1 = -12.65 + 0.65y;$ 
17:  $rlx_2 = 55.57 - 0.16x;$ 
18:  $rly_2 = -12.65 + 0.65y;$ 
19:  $rrx_1 = 227.55 - 0.37x;$ 
20:  $rry_1 = -73.91 + 1.13y;$ 
21:  $rrx_2 = 206.29 + 0.11x;$ 
22:  $rry_2 = -73.91 + 1.13y;$ 
    
```

error (MRE Eq. (2)) is evaluated, the absolute difference of each coordinate of the x and y axes between the ground truth and prediction because the prediction results have several differences with the ground truth. If the difference is within a specific range, it means it is correct within that range. In the experiment, the range used as a standard was 4 pixels.

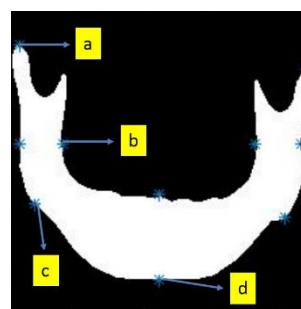


Figure. 2 Landmark mandibular point: (a) condyle, (b) ramus, (c) gonion, and (d) body of the mandible

Table 4. Evaluation

No	Landmark point	Mean Error (pixels)	SDR (%)
1	Left condyle	4	63.33
2	Right condyle	6	34.17
3	Left gonion	10	16.67
4	Right gonion	9	18.33
5	1st left ramus	7	32.50
6	2nd left ramus	7	25.83
7	1st right ramus	7	20.83
8	2nd right ramus	6	30.00
9	Bottom body	1	99.17
10	Upper body	6	50.00

For example, if the radial error is 3 pixels, it succeeds. Another way to evaluate is using the success detection rate (SDR Eq. (3)), where N_a shows the number of accurate detections, and N shows the total number of detections. We round up all measurement results. Table 4 is the evaluation result of determining mandibular landmark points on testing data (16 images).

Table 5. The results of the prediction of mandibular landmark points

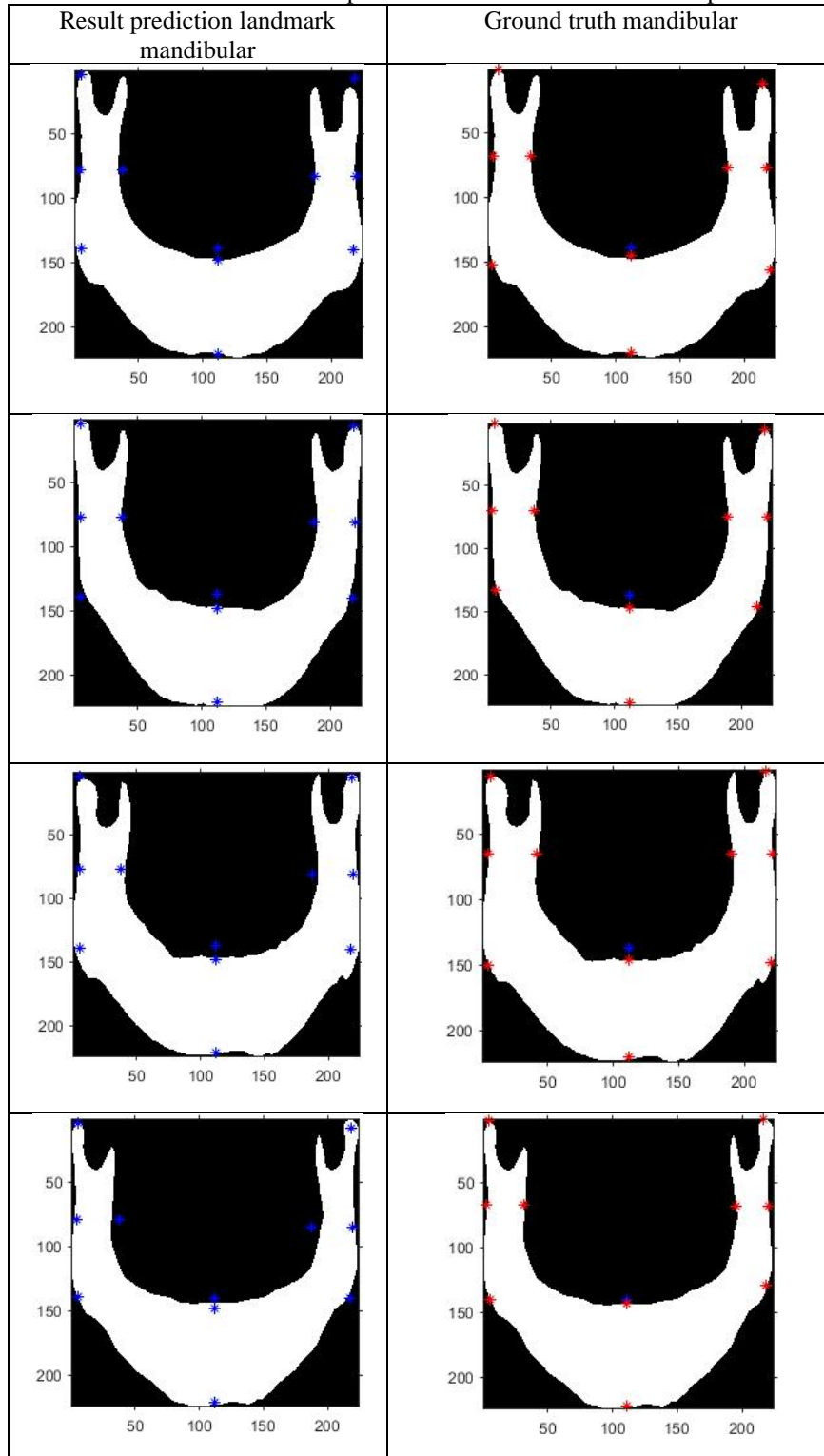
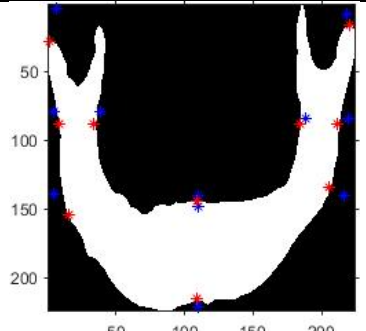
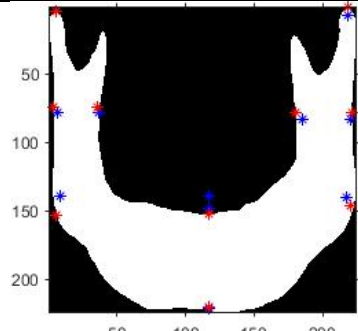
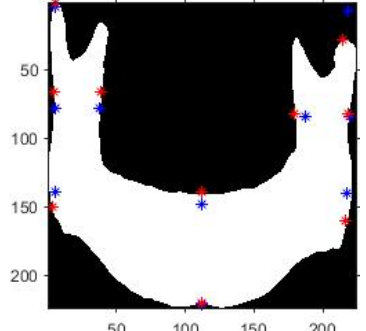
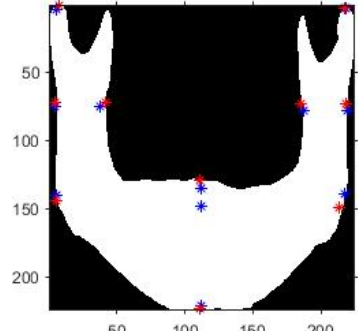
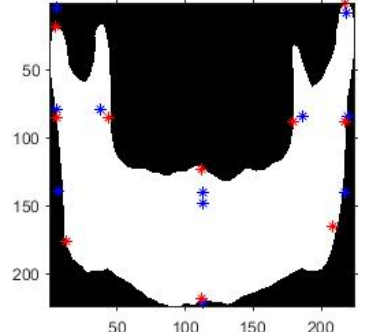
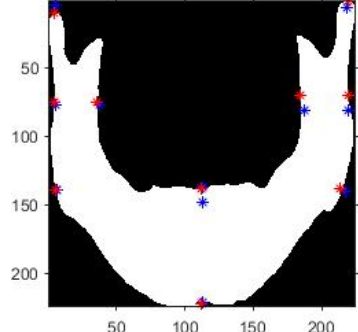
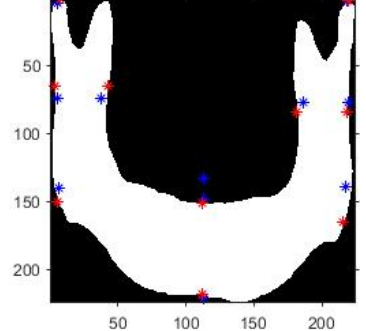
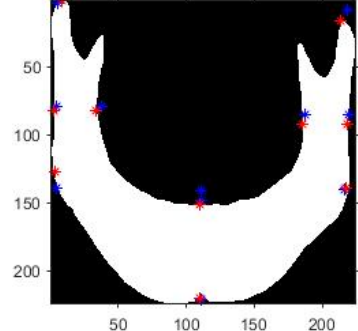
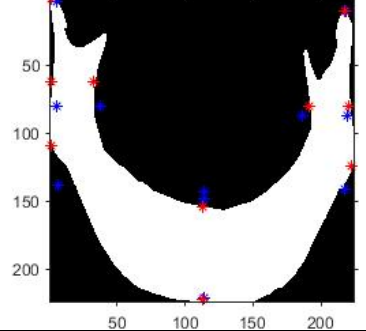
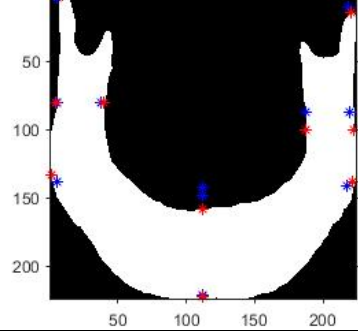
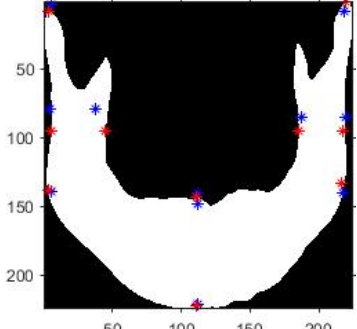
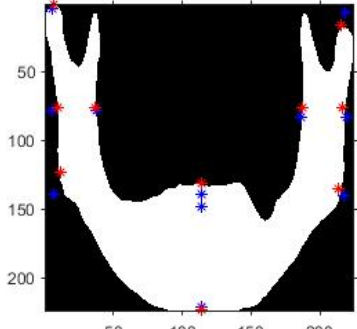
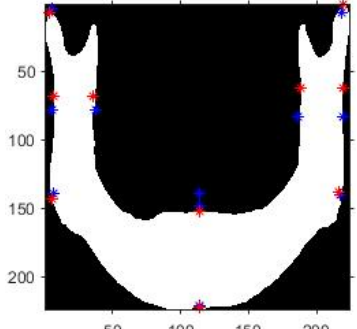
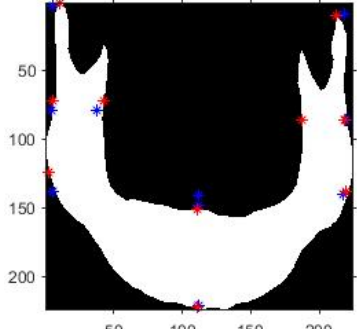
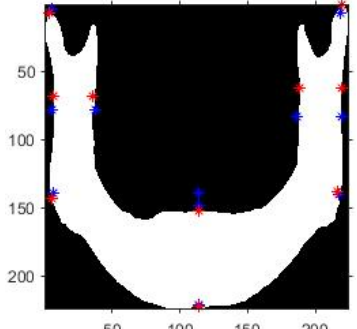
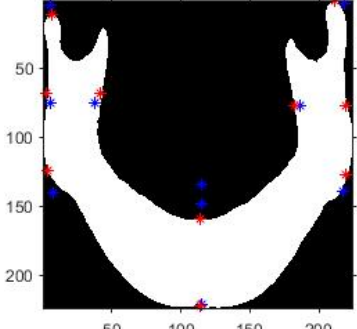
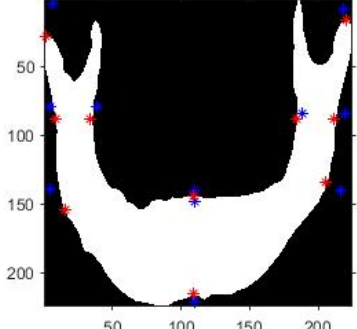
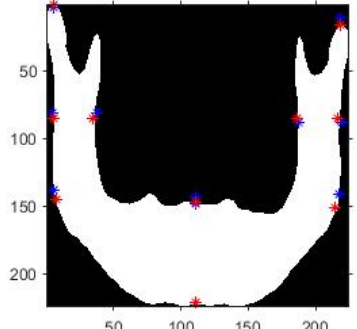
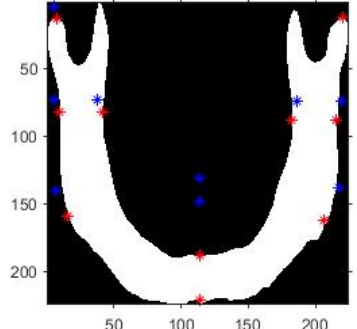
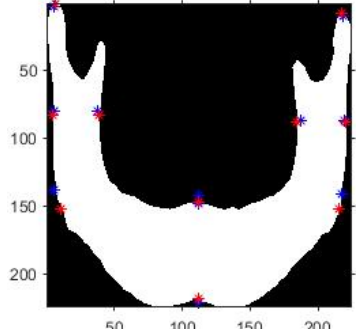


Table 6 describes several landmark points whose predictions are farthest from ground truth and closest to ground truth. In each figure in Table 6, the predicted landmark points are colored blue, while the ground truth landmark points are colored red. Table 6 shows the maximum distance between the predictions and the ground truth of each point and the

shortest distance between the predictions and the ground truth of each point. The prediction landmark point very far from the ground truth is the upper mandibular body point, which is 41 pixels, as shown in Fig. 3. In addition, the prediction landmark point far from the ground truth is the left gonion point, which is 38 pixels, as shown in Fig. 4. The results of

Table 6. Mandibular landmark point analysis

No	Landmark point	Max Error	Min Error
1	Left condyle		
2	Right condyle		
3	Left gonion		
4	Right gonion		
5	1st left ramus		

No	Landmark point	Max Error	Min Error
6	2nd left ramus	 <p>Max Error plot for the 2nd left ramus landmark point. The plot shows a white mandible silhouette on a black background. The y-axis is labeled from 50 to 200 (top to bottom), and the x-axis is labeled from 50 to 200 (left to right). Red and blue asterisks mark various points on the mandible. The plot shows the maximum error distribution for this landmark point.</p>	 <p>Min Error plot for the 2nd left ramus landmark point. The plot shows a white mandible silhouette on a black background. The y-axis is labeled from 50 to 200 (top to bottom), and the x-axis is labeled from 50 to 200 (left to right). Red and blue asterisks mark various points on the mandible. The plot shows the minimum error distribution for this landmark point.</p>
7	1st right ramus	 <p>Max Error plot for the 1st right ramus landmark point. The plot shows a white mandible silhouette on a black background. The y-axis is labeled from 50 to 200 (top to bottom), and the x-axis is labeled from 50 to 200 (left to right). Red and blue asterisks mark various points on the mandible. The plot shows the maximum error distribution for this landmark point.</p>	 <p>Min Error plot for the 1st right ramus landmark point. The plot shows a white mandible silhouette on a black background. The y-axis is labeled from 50 to 200 (top to bottom), and the x-axis is labeled from 50 to 200 (left to right). Red and blue asterisks mark various points on the mandible. The plot shows the minimum error distribution for this landmark point.</p>
8	2nd right ramus	 <p>Max Error plot for the 2nd right ramus landmark point. The plot shows a white mandible silhouette on a black background. The y-axis is labeled from 50 to 200 (top to bottom), and the x-axis is labeled from 50 to 200 (left to right). Red and blue asterisks mark various points on the mandible. The plot shows the maximum error distribution for this landmark point.</p>	 <p>Min Error plot for the 2nd right ramus landmark point. The plot shows a white mandible silhouette on a black background. The y-axis is labeled from 50 to 200 (top to bottom), and the x-axis is labeled from 50 to 200 (left to right). Red and blue asterisks mark various points on the mandible. The plot shows the minimum error distribution for this landmark point.</p>
9	Bottom body	 <p>Max Error plot for the Bottom body landmark point. The plot shows a white mandible silhouette on a black background. The y-axis is labeled from 50 to 200 (top to bottom), and the x-axis is labeled from 50 to 200 (left to right). Red and blue asterisks mark various points on the mandible. The plot shows the maximum error distribution for this landmark point.</p>	 <p>Min Error plot for the Bottom body landmark point. The plot shows a white mandible silhouette on a black background. The y-axis is labeled from 50 to 200 (top to bottom), and the x-axis is labeled from 50 to 200 (left to right). Red and blue asterisks mark various points on the mandible. The plot shows the minimum error distribution for this landmark point.</p>
10	Upper body	 <p>Max Error plot for the Upper body landmark point. The plot shows a white mandible silhouette on a black background. The y-axis is labeled from 50 to 200 (top to bottom), and the x-axis is labeled from 50 to 200 (left to right). Red and blue asterisks mark various points on the mandible. The plot shows the maximum error distribution for this landmark point.</p>	 <p>Min Error plot for the Upper body landmark point. The plot shows a white mandible silhouette on a black background. The y-axis is labeled from 50 to 200 (top to bottom), and the x-axis is labeled from 50 to 200 (left to right). Red and blue asterisks mark various points on the mandible. The plot shows the minimum error distribution for this landmark point.</p>

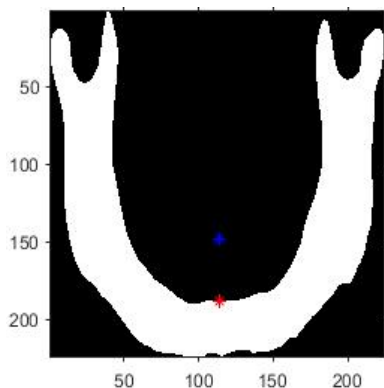


Figure. 3 Landmark points of the upper mandible body (red ground truth, blue prediction)

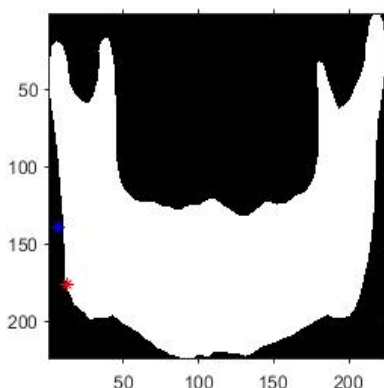


Figure. 4 Landmark points of the left gonion body (red ground truth, blue prediction)

Table 7. Performance method

Method	SDR (%)				
	2 mm	2.5 mm	3 mm	4 mm	4 pixel
Deep Regression [19]	82.99	88.52	92.55	96.50	-
CephaNet [20]	77.45	81.18	84.48	88.25	-
Deep Learning [21]	62.00	70.50	78.10	86.60	-
DCNN [22]	87.51	91.83	94.74	98.01	-
Linear Regression (Our)	-	-	-	-	39.08

the projection of landmark points far from the ground truth are due to the different shapes of the ramus and width of the mandible, so the position of the coordinates (x, y) of the gonion and upper body of the mandible is not correct. In Table 7, research [19-22] uses cephalometric images, and the number of predicted landmark points is 19. The evaluation method uses standard limits of 2 mm, 2.5 mm, 3 mm, and 4 mm. Our proposal uses a 4-pixel standard because 1 mm is 3.78 pixels, and the evaluation results are very low, namely 39.08%. We used

panoramic dental radiographic images, and ten mandibular landmark points were predicted using the Linear Regression method.

6. Conclusion

This study proposes a linear regression method to generate mandibular landmarks on panoramic radiographs automatically. There are predicted to be ten mandibular landmark points, including two condyle, two gonion, four ramus, and two body of the mandible. From our proposal, the left gonion landmark point does not match the data from radiologists, with the lowest SDR value of 16.67%. On the other hand, the best landmark point is the bottom point of the body landmark because the highest SDR result is 99.17%.

Further research suggests improving how to method generate the mandibular landmark points on the gonion that have a low error difference from the actual data from doctors.

Conflicts of interest

The authors declare no conflict of interest.

Author contributions

Conceptualization: Nur Nafiiyah, Chastine Faticah; methodology: Nur Nafiiyah, Chastine Faticah; software, Nur Nafiiyah; validation, Chastine Faticah, Darlis Herumurti, Eha Renwi Astuti, and Ramadhan Hardani Putra; resources data, Eha Renwi Astuti, Ramadhan Hardani Putra; writing—original draft preparation: Nur Nafiiyah; writing—review and editing: Nur Nafiiyah, Chastine Faticah, Darlis Herumurti, Eha Renwi Astuti, Ramadhan Hardani Putra, and Agus Subhan Akbar.

Acknowledgments

Thanks to Deputy for Strengthening Research and Development, Ministry of Research and Technology/National Research and Innovation Agency, Indonesia, for providing research funding through the Doctoral Dissertation Research scheme with research contract number 1255/PKS/ITS/2020. Thanks to the Dental and Oral Hospital of Universitas Airlangga, Surabaya providing dental radiographic panoramic data.

References

[1] F. Fan, W. Ke, W. Wu, X. Tian, T. Lyu, Y. Liu, P. Liao, X. Dai, H. Chen, and Z. Deng, "Automatic human identification from panoramic dental radiographs using the convolutional neural network",

- Forensic Sci. Int.*, Vol. 314, 2020, doi: 10.1016/j.forsciint.2020.110416.
- [2] C. Muramatsu, T. Morishita, R. Takahashi, T. Hayashi, W. Nishiyama, Y. Ariji, X. Zhou, T. Hara, A. Katsumata, E. Ariji, and H. Fujita, "Tooth detection and classification on panoramic radiographs for automatic dental chart filing: improved classification by multi-sized input data", *Oral Radiol.*, Vol. 37, No. 1, 2021, doi: 10.1007/s11282-019-00418-w.
- [3] H. Chen, C. Sun, P. Liao, Y. Lai, F. Fan, Y. Lin, Z. Deng, and Y. Zhang, "A fine-grained network for human identification using panoramic dental images", *Patterns*, Vol. 3, No. 5, p. 100485, 2022, doi: 10.1016/j.patter.2022.100485.
- [4] D. Milošević, M. Vodanović, I. Galić, and M. Subašić, "Automated estimation of chronological age from panoramic dental X-ray images using deep learning", *Expert Syst. Appl.*, Vol. 189, 2022, doi: 10.1016/j.eswa.2021.116038.
- [5] M. A. A. Aman, A. Sarkar, M. Dutt, and A. Biswas, "A linear time combinatorial algorithm to compute the relative orthogonal convex hull of digital objects", *Theor. Comput. Sci.*, Vol. 847, 2020, doi: 10.1016/j.tcs.2020.09.043.
- [6] L. Fang, N. Liang, W. Kang, Z. Wang, and D. D. Feng, "Real-time hand posture recognition using hand geometric features and Fisher Vector", *Signal Process. Image Commun.*, Vol. 82, 2020, doi: 10.1016/j.image.2019.115729.
- [7] P. T. An, P. T. T. Huyen, and N. T. Le, "A modified Graham's convex hull algorithm for finding the connected orthogonal convex hull of a finite planar point set", *Appl. Math. Comput.*, Vol. 397, 2021, doi: 10.1016/j.amc.2020.125889.
- [8] A. P. Nemirko and J. H. Dulá, "Machine learning algorithm based on convex hull analysis", in *Procedia Computer Science*, Vol. 186, 2021, doi: 10.1016/j.procs.2021.04.160.
- [9] M. G. Tsipouras, N. Giannakeas, A. T. Tzallas, Z. E. Tsianou, P. Manousou, A. Hall, I. Tsoulos, and E. Tsianos, "A methodology for automated CPA extraction using liver biopsy image analysis and machine learning techniques", *Comput. Methods Programs Biomed.*, Vol. 140, 2017, doi: 10.1016/j.cmpb.2016.11.012.
- [10] W. G. Flores and J. H. López, "Assessment of the invariance and discriminant power of morphological features under geometric transformations for breast tumor classification", *Comput. Methods Programs Biomed.*, Vol. 185, 2020, doi: 10.1016/j.cmpb.2019.105173.
- [11] Y. Faradhilla, A. Z. Arifin, N. Suciati, E. R. Astuti, R. Indraswari, and M. Widiarsi, "Residual Fully Convolutional Network for Mandibular Canal Segmentation", *Int. J. Intell. Eng. Syst.*, Vol. 14, No. 6, 2021, doi: 10.22266/ijies2021.1231.20.
- [12] A. Fariza, A. Z. Arifin, E. R. Astuti, and T. Kurita, "Segmenting tooth components in dental X-ray images using Gaussian kernel- based conditional spatial Fuzzy C-Means clustering algorithm", *Int. J. Intell. Eng. Syst.*, 2019, doi: 10.22266/IJIES2019.0630.12.
- [13] J. P. Pillai, R. J. Shah, B. Darji, A. Banker, and R. J. Pillai, "Association of the gonial angle with age, gender, and dental status: A radiographic study using lateral cephalogram and orthopantomogram", *J. Forensic Radiol. Imaging*, 2018, doi: 10.1016/j.jofri.2018.11.002.
- [14] V. Sairam, G. Potturi, B. Praveen, and G. Vikas, "Assessment of effect of age, gender, and dentoalveolar changes on mandibular morphology: A digital panoramic study", *Contemp. Clin. Dent.*, 2018, doi: 10.4103/ccd.ccd_704_17.
- [15] S. Pillay, S. Ishwarkumar, B. D. Gama, and P. Pillay, "The Morphometry of the Angle of Mandible and its Correlation with Age and Sex in the eThekweni Metropolitan Region: A Panoramic Study", *Int. J. Morphol.*, Vol. 35, No. 2, 2017, doi: 10.4067/s0717-95022017000200045.
- [16] J. Leversha, G. McKeough, A. Myrteza, H. S. Wakefield, J. Welsh, and A. Sholapurkar, "Age and gender correlation of etgonial angle, ramus height and bigonial width in dentate subjects in a dental school in Far North Queensland", *J. Clin. Exp. Dent.*, Vol. 8, No. 1, 2016, doi: 10.4317/jced.52683.
- [17] A. Okkesim and T. S. Erhamza, "Assessment of mandibular ramus for sex determination: Retrospective study", *J. Oral Biol. Craniofacial Res.*, Vol. 10, No. 4, pp. 569–572, 2020, doi: 10.1016/j.jobcr.2020.07.019.
- [18] N. V. Blanco, P. V. Quintana, Á. A. Ardao, I. Tomás, and M. J. Carreira, "Automated description of the mandible shape by deep learning", *Int. J. Comput. Assist. Radiol. Surg.*, Vol. 16, No. 12, pp. 2215–2224, 2021, doi: 10.1007/s11548-021-02474-2.
- [19] Z. Zhong, J. Li, Z. Zhang, Z. Jiao, and X. Gao, "An Attention-Guided Deep Regression Model for Landmark Detection in Cephalograms", *Lecture Notes in Computer Science (including subseries Lecture Notes in Artificial Intelligence and Lecture Notes in Bioinformatics)*, Vol. 11769 LNCS, 2019, doi: 10.1007/978-3-030-32226-7_60.
- [20] J. Qian, M. Cheng, Y. Tao, J. Lin, and H. Lin, "CephaNet: An improved faster r-cnn for cephalometric landmark detection", In: *Proc. of International Symposium on Biomedical Imaging*, Vol. 2019-April, 2019, doi: 10.1109/ISBI.2019.8759437.
- [21] Y. Song, X. Qiao, Y. Iwamoto, and Y. W. Chen, "Automatic Cephalometric Landmark Detection on X-ray images using a deep-learning method", *Appl. Sci.*, Vol. 10, No. 7, 2020, doi: 10.3390/app10072547.
- [22] L. Wang, L. Ma, Y. Li, K. Niu, and Z. He, "A DCNN system based on an iterative method for automatic landmark detection in cephalometric X-ray images", *Biomed. Signal Process. Control*, Vol. 68, 2021, doi: 10.1016/j.bspc.2021.102757.
- [23] C. W. Wang, C. T. Huang, J. H. Lee, C. H. Li, S. W. Chang, M. J. Siao, T. M. Lai, B. Ibragimov, T.

Vrtovec, O. Ronneberger, P. Fischer, T. F. Cootes, and C. Lindner, "A benchmark for comparison of dental radiography analysis algorithms", *Med. Image Anal.*, Vol. 31, 2016, doi: 10.1016/j.media.2016.02.004.

- [24] H. Lee, M. Park, and J. Kim, "Cephalometric landmark detection in dental x-ray images using convolutional neural networks", In: *Proc. of Medical Imaging 2017: Computer-Aided Diagnosis*, Vol. 10134, 2017, doi: 10.1117/12.2255870.
- [25] N. Nafi'iyah, C. Fatichah, D. Herumurti, E. R. Astuti, and R. H. Putra, "MobileNetV2 Ensemble Segmentation for Mandibular on Panoramic Radiography", *Int. J. Intell. Eng. Syst.*, Vol. 16, No. 2, 2023, doi: 10.22266/ijies2023.0430.45.
- [26] D. P. Mohite, M. S. Chaudhary, P. M. Mohite, and S. P. Patil, "Age assessment from mandible: Comparison of radiographic and histologic methods", *Rom. J. Morphol. Embryol.*, Vol. 52, No. 2, pp. 659–668, 2011.